2011

Pool Boiling Performance Comparison of Smooth and Sintered Copper Surfaces with and without Carbon Nanotubes

John P. McHale
Purdue University

S V. Garimella
Purdue University, sureshg@purdue.edu

Timothy S. Fisher
Purdue University

Glen A. Powell
Purdue University

McHale, John P.; Garimella, S V.; Fisher, Timothy S.; and Powell, Glen A., "Pool Boiling Performance Comparison of Smooth and Sintered Copper Surfaces with and without Carbon Nanotubes" (2011). *CTRC Research Publications.* Paper 156.
http://dx.doi.org/10.1080/15567265.2011.575918

Pool boiling performance comparison of smooth and sintered copper surfaces with and without carbon nanotubes

John P. McHale, Suresh V. Garimella*, Timothy S. Fisher, and Glen A. Powell
Cooling Technologies Research Center and Birck Nanotechnology Center
School of Mechanical Engineering
Purdue University, West Lafayette, IN 47907-2088 USA

ABSTRACT

Pool boiling heat transfer is measured with two individual working fluids on copper surfaces enhanced with sintered copper powder and carbon nanotubes. The working fluids are a segregated hydrofluoroether, HFE-7300, and deionized water. The surfaces considered in the experiments include smooth copper, copper with sintered copper particles, smooth copper with copper-coated carbon nanotubes (CNT), and copper with sintered copper particles and copper-coated carbon nanotubes. Characteristics of the resulting boiling curves are discussed and analyzed. Lower wall superheats resulted from both the sintered particles and the CNT array for both working fluids. For water, there was no additional benefit from the addition of CNTs on the sintered particle substrate. For HFE-7300, however, the hybrid (sintered with CNTs) surface achieved the lowest wall superheat at high heat fluxes. Critical heat flux for HFE-7300 increased by more than 45% for the hybrid surface relative to the smooth copper surface.

Keywords: enhanced boiling, porous surface, carbon nanotube, biporous wick, surface morphology, sintered surface, thermosyphon

* Corresponding author, Phone: 765-494-5621, sureshg@purdue.edu

1 INTRODUCTION

Surface enhancements are often employed in boiling systems to reduce wall superheat and/or to increase the critical heat flux. In electronics cooling applications and heat pump cycles, for example, surface temperature changes as small as a few degrees can make a significant difference in overall system performance. In this study, pool boiling performance at atmospheric pressure is investigated for sintered copper surfaces employing carbon nanotubes (CNTs) to enhance the surface structure. Boiling curves for these engineered surfaces are reported and compared with those for smooth surfaces as well as with results in the literature.

It is well known that the presence of surface defects enhances boiling heat transfer. Hsu [1] first derived a relationship for the size range of active nucleating cavities on a boiling surface. Various approaches to modification of metallic surfaces for improved boiling performance have consequently been developed in the literature. Webb [2] summarized boiling curves obtained for porous metal coatings in past studies, and highlighted a rule of thumb that the best boiling performance for sintered surfaces was achieved at $\delta/d_p = 4$. He also proposed that size of the pore, rather than of the particle as had been previously postulated, was the critical modeling parameter. Czikk and O'Neill [3] formulated a model for boiling within porous coatings made of connected spherical microparticles. However, Webb [2] recommended the Nishikawa [4] correlation instead, based on a comparison with existing experimental boiling data. He also recommended employing measured porosity value rather than the theoretical value ($\varepsilon = 0.476$) based on a square-packing arrangement. Afgan *et al.* [5] studied pool boiling of distilled water, R-113 and ethanol from horizontal tubes of 3 to 18 mm diameter, coated with sintered metal layers formed of spherical or dendritic particles. Pool boiling tests were conducted over a wide range of heat fluxes, extending well beyond the dryout point. They found pronounced

hysteresis to occur in some tests, also noting that times to reach steady state were in some cases as long as a few hours. They attributed the long settling times to the development of a final liquid-vapor structure within the porous matrix. Boiling hysteresis was observed only for coating thicknesses over 1 mm for water. For the highly wetting fluids R-113 and ethanol, hysteresis was observed for all coating thicknesses. Afgan *et al.* proposed that the heat transfer exponent n (where $q''_w \propto \Delta T_w^n$) is an indicator of the vapor behavior in different parts of the boiling curve. For $n > 1$, typical of the nucleate boiling regime for water, the number of active nucleation sites increases with q''. For $n \approx 1$, the thickness of the vapor layer within the porous structure is constant. Finally, for $n < 1$, as observed in transition regions for the wetting liquids, the thickness of the vapor layer increases with ΔT_w. Ramaswamy *et al.* [6,7] studied pool boiling of FC-72 from multi-layered copper and silicon surfaces with interconnected pores formed by cross-cutting microchannels on opposing sides of each layer. They found that: 1) increasing the pore size increased the heat transfer coefficient for low to moderate heat fluxes; 2) decreasing the pore pitch increased the heat transfer coefficient for all heat fluxes; and 3) by varying the number of layers between 1 and 6, the heat transfer coefficient was not substantially changed in the fully developed boiling regime.

Critical heat flux on porous coated surfaces has also been investigated in the literature. Liter and Kaviany [8] proposed to increase CHF by structuring the boiling surface in such a way that the Rayleigh-Taylor instability wavelength would be fixed. Vapor jets would be prevented from forming with a pitch equal to the natural least stable wavelength $\lambda_{crit} = 2\pi\sqrt{\sigma / g(\rho_l - \rho_v)}$, thus improving the hydrodynamics of countercurrent liquid-vapor flow near the surface. Their surfaces were composed of sintered copper spheres so that liquid availability at the surface and the thermal "activity" (see [9,10]) of the heated surface would not be limiting parameters in the

critical heat flux condition. Porous evaporators with space allotted for vapor flow were also proposed by Wu *et al.* [11], among others. Recent work by Alexander and Wang [12] emphasizes the difficulty of engineering separate liquid and vapor flow paths.

Boiling heat transfer may also be enhanced by employing multiple capillary length scales. Carbon nanotubes (CNTs) have been employed in this regard. Where the porous matrix often has a capillary radius on the order of 100 μm, CNT-based nanostructures can provide capillary radii on the order of a few hundred nm. Park and Jung studied the pool boiling of refrigerants [13] and deionized water [14] with and without the addition of 1% by volume CNTs to the fluids, using acid treatment to prevent CNT agglomeration. They found heat transfer enhancement due to the addition of CNTs to occur primarily at lower heat fluxes and reported that surface fouling did not occur. With the addition of a polymer dispersant [15], however, the heat transfer coefficients decreased, but critical heat flux values increased substantially due to deposition of CNTs on the surface. Khanikar *et al.* [16] studied flow boiling on smooth copper and CNT-coated copper surfaces. SEM images revealed that the structure of the CNT coating changed after dryout occurred at high mass fluxes, resulting in a 30% decrease in CHF. Launay *et al.* [17] studied pool boiling of water and PF-5060 (FC-72) from silicon surfaces with different types of surface enhancements, including multiwall carbon nanotubes (MWCNTs). They found that CNT micro- and nanostructures enhanced heat transfer at low to moderate heat fluxes, but also significantly reduced critical heat flux. They made the important conjecture that both the increase in h and the decrease in q''_{CHF} resulted from a reduction in the wettability of the surface. Ujereh *et al.* [18], using FC-72 as a working fluid, showed that: 1) CNT coatings form effective vapor traps that drastically reduce incipience superheat; 2) increasing the coating coverage area improved the heat transfer coefficient monotonically; and 3) CNT coatings may reduce CHF for

microstructured surfaces if the array density is high enough. Ahn *et al.* [19] showed that carbon nanotube arrays can increase critical heat flux, heat transfer coefficient in both nucleate and film boiling regimes, and minimum heat flux (MHF) in film boiling. They proposed that CNTs longer than the minimum sustainable vapor film thickness may disrupt the establishment of vapor films on the surface, and may enhance thermal conductivity across the vapor film after dryout. Kim *et al.* [20] recently applied an evaporated copper layer to coat carbon nanotubes grown on a screen mesh in order to make the CNTs hydrophilic. They found that higher levels of positive bias on the substrate during CNT growth and greater metallization coating thicknesses improved evaporative heat transfer. Hashimoto *et al.* [21] developed a water vapor chamber heat spreader utilizing sintered copper particles covered by CNTs on the evaporator surface, and UV radiation was used to render the CNT arrays hydrophilic. Their results showed that the overall thermal resistance of the heat spreader package was most reduced for the longest and densest CNT arrays.

The following conclusions can be drawn from the studies discussed above. The pool boiling performance of microporous surfaces is strongly tied to how the liquid and vapor interfaces form and move within the microstructure. The inherent heat transfer advantages of microstructured boiling surfaces may be further augmented by the addition of nanostructures such as CNTs. The wettability and capillarity effects of CNT arrays may be among their most important features for evaporative heat transfer. CNT arrays have been speculated to act as permanent vapor traps, reducing or eliminating the boiling incipience superheat for various surface structures. The combination of CNTs as nanoscale wick structures superposed on existing microscale porous structures may successfully increase heat transfer coefficients and critical heat flux values for a variety of working fluids. However, it is unclear whether the

effects of CNTs on nucleate boiling heat transfer are attributable to wetting and wicking effects or to gross area enhancement. Additionally, the flow boiling results of Khanikar *et al.* [16] highlight the possibility that under some boiling circumstances, dryout may detrimentally alter the structure of a CNT surface. In the present work, the effects of wettability and area enhancement on boiling heat transfer and critical heat flux are investigated. Experimental boiling curves with ascending and descending heat flux are investigated and analyzed for three different enhanced surface structures and a bare copper surface.

2 TEST PIECE FABRICATION

The four test pieces for this work were all fabricated by preparing the surface on a 25.4-mm by 25.4-mm by 1.0 mm thick pure (99.99%) copper sheet and then soldering (Sn/Pb/Ag/Sb 62/35.75/2/0.25) to a test block of the same pure copper material. The surface preparation is described below; further details are provided in [22]. The bare copper sheet was of unpolished mill-grade finish prior to enhancement.

The bare copper surface was successively degreased in acetone and methanol baths to remove machining oils, and then cleaned in a standard piranha solution of 3 parts H_2SO_4 (96%) to 1 part H_2O_2 (30%) for at least 5 minutes to remove any inorganic materials.

For preparing the sintered copper surface shown in Figure 1(a), spherical copper particles (Alfa Aesar 42623, 99.9% pure) were sieved with 140- and 170-mesh screens to produce a uniform particle size of 90-106 μm. The particles were then poured into a ceramic mold placed on top of the 1-mm thick degreased copper substrate. The assembly was heated in a quartz-tube furnace at 950 °C under a forming gas atmosphere (N_2 with 5.7% H_2 by mass) to prevent oxidation. The thermal cycle included a 30-minute room temperature purge, followed by a 30-minute ramp up to the sintering temperature, 950 °C, a 60-minute soak at 950 °C, and a 150-

minute ramp down to 50 °C, at which point the sample was removed from the oven. The porosity of the sintered layer, obtained by weight and volume measurements, was 65%.

Growth of a dense, vertically aligned array of multi-walled (MW) CNTs on a catalyzed copper substrate [as shown in Figure 1(b)] was achieved by microwave-plasma chemical vapor deposition (MPCVD) using H_2 and CH_4 feed gases. CNT growth was catalyzed with a "trilayer" evaporated metal surface coating consisting of a 60-nm Ti adhesion layer, a 10-nm Al film to promote catalyst particle formation, and a 3-nm Fe catalyst layer [23]. The MPCVD process was conducted for 10 minutes under a partial vacuum at a temperature of 900 °C; under such conditions the iron layer breaks up into nanoparticles [24], seeding dense growth of CNTs. The median length of the CNTs resulting from this process was approximately 40 μm. Following growth, the hydrophobic CNTs were rendered hydrophilic by e-beam evaporative deposition of pure copper. The copper layer was found by scanning electron microscopy to coat the CNTs conformally over approximately the top 10 μm of their length. The conformal coating of approximately 20 nm thickness increased the nanotube diameter from 50 nm as grown to 90 nm after coating.

The fourth test surface consisted of a CNT array grown on sintered copper spheres, as shown in Figure 1(c). The catalyst in this case was a polymer dendrite structure [25], combined in solution with ferric chloride hexahydrate ($FeCl_3 \cdot 6H_20$). The sintered surface was first coated with 100-nm Ti adhesion layer which also acted as a diffusion barrier. The catalyst solution was then applied uniformly to the test surface by airbrushing with multiple passes. The surface was then heated at 150 °C to remove volatile components and to drive off water from the hydrate. The subsequent CNT growth by MPCVD and metallization were as described above. The quality of CNT arrays grown by this method was not as good as for the trilayer-catalyzed

array on the flat surface in terms of uniformity and apparent defects indicated by kinks in the nanotubes. The median length of CNTs for this surface, as determined from SEM images, was approximately 10 μm, and each sphere's surface was only about 80% covered. The metallization layer, however, conformally coated the entire length of the CNTs as far as was visible by the SEM.

3 EXPERIMENTAL METHOD

The experimental facility for the boiling tests and the data collection are described in detail in McHale and Garimella [26], and are summarized here along with a description of the modifications made for the present work. A diagram of the experimental facility is shown in Figure 2. Each heater block, measuring 25.4 mm x 25.4 mm x 36.6 mm, is fabricated of oxygen-free copper. Twelve embedded cartridge heaters in the block provide an evenly distributed heat flux to the boiling surface. The surface temperature is extrapolated from the temperatures measured at the thermocouple locations. The heat input to the test block is measured by recording the DC voltage and current to the cartridge heaters. The pool is vented through a cold vapor trap to the atmosphere; all experiments are therefore carried out at atmospheric pressure.

The copper test surfaces described in the previous section are soldered to one of four identical copper heater blocks using a low-melting indium-tin solder with a bond line thickness of 100 μm. The sample is bathed in argon gas during the soldering process, ensuring minimal oxidation of the surface.

3.1 Heat loss calculation

While the heat flux through the test surface may be calculated directly from the thermocouple measurements, lower experimental uncertainties are achieved if the heat flux is determined according to the following relation:

$$q''_w = \frac{q_{in} - q_{loss}}{A_{base}} \tag{1}$$

where the value of q_{loss} is determined from a numerical model implemented in the commercial software package FLUENT [27]. The problem geometry was fully represented in three-dimensions, and the results confirmed to be grid-independent through simulations using several mesh densities. The heat loss is calculated based on multivariate regression of the numerical results using a block thermal conductivity $k_s = 385$ W/m·K [28] and an external convection coefficient set by matching the experimentally measured heat loss for $\Delta T_w = 0$. Regression functions were developed using Engineering Equation Solver (EES) [28]. The ambient air temperature T_∞ was found to have a small effect on the calculated heat loss and was included in the heat loss regression equation:

$$q_{loss}\ (\mathrm{W}) = -44.616 - 6.095\times10^{-2} T_\infty + 1.033\times10^{-2} q_{in} + 1.814\times10^{-1} T_w \tag{2}$$

where the unit of temperature is K. The influence of ambient temperature is small compared to the other two variables since the range of T_∞ is only about 5 K, while the range of q_{in} is more than 100 W and that of T_w up to 40 K. Heat fluxes in the fully developed nucleate boiling regime and higher are of primary interest in this study so that the input power and wall temperature are the key determinants of heat loss.

3.2 Experimental uncertainties

The calibrated thermocouple uncertainty is estimated to be 0.3 K based on the amplitude of noise in the experimental data. The thermocouple reference junction temperature measured with a high-accuracy RTD is within less than 0.1 K and does not add appreciably to the uncertainty. The test surface temperature uncertainty is as much as 0.6 K due to the additional uncertainties of thermocouple location and solder bond thickness. Jones and Garimella [29] found the uncertainty in heat loss for this facility to be only 1-2% of the total power dissipation at heat fluxes above 12 W/cm^2. The uncertainty in heat loss due to use of the regression equation (2) is negligible compared to the uncertainty associated with parameters used as inputs to the numerical simulation.

4 RESULTS AND DISCUSSION

The results of the pool boiling experiments are described in the following subsections. General aspects of the boiling curves, including comparisons between fluids and surfaces, are explained. Reasons are provided for the observed heat transfer behavior through first-order analyses. Morphological changes in the CNT-enhanced boiling surfaces due to thermal testing are also described.

4.1 Boiling curves

Pool boiling curves for the four surfaces are compared in Figures 3 and 4 with HFE-7300 and DI water, respectively. The open symbols refer to the ascending boiling curve (heat flux increasing), while the downward-pointing triangles refer to the descending curve. Measured critical heat flux points are marked with the symbol "×". The boiling curves for HFE-7300 were limited to a heat flux of 27 W/cm^2 due to the condenser flow limit (see Figure 3), while one

boiling curve for water was limited to 55 W/cm^2 because of difficulties with the cooling equipment.

The sintered surfaces exhibit better boiling performance (lower ΔT_w) for lower heat fluxes. The CNT-enhanced flat surface outperforms the bare flat surface for both working fluids. The presence of CNTs on the sintered surface provide no additional benefit in water, but do achieve a significant performance enhancement in HFE-7300 over both the traditional sintered surface and the CNT-enhanced flat surface. Specific features of the boiling curves are discussed in greater detail in the following.

4.2 Boiling incipience

Boiling incipience temperatures varied greatly for the surfaces studied, as summarized in Table 2. Incipience of boiling from enhanced surfaces is always associated with the trapping of either vapor or noncondensible gas on the surface. The bubble embryo radius for each incipience temperature condition was calculated based on the standard application of the Young-Laplace and Clausius-Clapeyron equations [30] in order to demonstrate the trapping effectiveness of the surface. Incipience temperatures were always lower for water than for HFE-7300. Other observations include:

(1) the application of carbon nanotubes to a flat surface reduces boiling incipience temperatures, significantly reducing the temperature excursion common for a highly wetting liquid;

(2) the comparatively large-scale sintered coating is more effective than carbon nanotubes at reducing the incipience temperature;

(3) the hybrid surface virtually eliminated the incipience temperature for the highly wetting HFE-7300; however, in water there was no apparent incipience benefit for the hybrid

surface over the conventional sintered surface, largely because the incipience superheat was less than 1K for both.

Previous authors [31-35] considered mechanisms by which noncondensable gas could be trapped on a surface, thereby providing two-phase interfaces for heterogeneous nucleation. Hsu's nucleation theory requires a finite wall superheat for the incipience of bubble growth to occur according to the limiting thermal boundary layer thickness in the superheated liquid. Afgan, *et al.* [5] suggested that for thermally conductive porous heated layers, Hsu's maximum cavity radius criterion is not applicable, since the superheated fluid within the matrix is likely to be surrounded by the heated solid at T_w. We note, however, that the boundary layer thickness is quite large (on the order of 1 mm) for the single-phase natural convection condition experienced prior to boiling incipience in the present work. In this case, only Hsu's minimum radius criterion is important. As shown in Table 2, the minimum bubble radius depended on the pore size of the surface, and also on the wettability of each fluid.

Highly wetting liquids require low-angle cavities for gas trapping to occur (see, e.g., Reed and Mudawar [36]). Ujereh *et al.* [18] suggested that carbon nanotube arrays provide effective cavity angles near zero. The sintered copper surfaces both with and without CNTs in the present work, however, had incipience superheats much lower than the CNT-enhanced flat surface. We therefore conclude that the gas- or vapor-trapping capability of a sintered copper layer produces larger bubble embryos than CNTs alone. Addition of CNTs to the sintered layer, however, allows embryos 8 times larger to be trapped for the highly wetting HFE-7300. This is not the case for water, for which the maximum trapped bubble size in the sintered layer already approaches the pore length scale.

4.3 Boiling hysteresis

Three main types of hysteresis were present in the boiling curves: *incipient boiling* hysteresis, *long time constant* hysteresis, and apparent hysteresis from contamination. First, spreading incipience of boiling (see, e.g., Jones, *et al.* [37]) caused a vertical slope in the ascending heat flux curve for the CNT-enhanced flat surface for both fluids. The descending curve, with all possible sites active, followed a smooth path with a monotonically changing slope. This was also the case for the plain surface with water as the working fluid.

Second, very long time constants were apparent in boiling from the traditional sintered surface, primarily for HFE-7300, but also to some extent for water. This type of hysteresis was relatively independent of heat flux and more pronounced for higher wall superheats. For example, two successive data points in Figure 3 at the same heat flux, 17 W/cm^2, were collected about 1 hour apart for the descending boiling curve of HFE-7300 on the sintered copper surface (for flat surfaces in the present experimental apparatus, 5 to 10 minutes is known to be sufficient time for steady state). The wall superheat for the second data point decreased by more than 1 K from the first. Afgan *et al.* [5] reported this type of hysteresis in their boiling curve, observing some of their data points to shift in temperature, depending upon how much time was allowed for the system to equilibrate. They attributed the shift to the presence of vapor within the porous layers, and pointed out that thin layers with high "permeability" did not exhibit any hysteresis.

Third, contamination of the bare copper surface during boiling of HFE-7300 resulted in an apparent hysteresis in the curve. Contamination was not observed with either water or FC-77 (tested in prior experiments [37]). In the HFE, boiling performance deteriorated with time and is manifested as a progressive shift of the nucleate boiling curve to the right; in successive tests, the curve experienced little change in CHF but the wall superheat in boiling increased by a total

of approximately 4.5 K. None of the enhanced surfaces experienced such a wall superheat shift over time. A series of surface and fluid tests revealed that the contaminant was likely a phthalate oil (normal boiling point ~380 °C) extracted from Viton o-rings or Tygon-type flexible tubing in the facility. HFEs are well known to be active solvents and are in fact routinely used for cleaning electronic components because of the high solubility of certain processing residues in HFE. It is believed that the mechanism of performance decrease was the deposition of oil in the cavities on the surface, causing permanent nucleation site deactivation. Since the enhanced surfaces all contain an overabundance of potential nucleation sites, deactivation of some percentage would not have any observable effect. All data presented in this work are those of the first test for each sample with each data point taken at our standard criterion for steady state, which is a strict observance of $dT_w/dt \leq 0.006\,°\text{C/min}$.

4.4 Boiling curve crossover

Boiling curves for the sintered surfaces in three out of the four cases crossed over the curves for the flat surfaces and exhibited higher wall superheats at high heat fluxes. It is interesting to note that the boiling curves did not cross only for HFE-7300 on the hybrid (CNT+sintered) surface.

Boiling incipience occurs at near-zero superheat for the porous surfaces. The boiling curve correlation exponent *n*, where $q''_w \propto (\Delta T_w)^n$, is less than or equal to 1 for these surfaces, in contrast to the expected value of 2 to 3 for flat surfaces. This can be explained by the growing thermal resistance of an expanding dried-out volume at the base of the sintered layer [5].

For the sintered Cu coatings, $\delta / d_p \approx 10$, and on average about 13-14 particles lie in the heat flow path from the substrate to the top of the porous layer. Thermal resistance calculations based on the geometric measurements and material properties suggest that the measured value of

$\Delta T_{w,CHF}$ would be on the order of 10 K higher for such a "thick" porous coating than for a plain copper surface, assuming the same local boiling curve. Indeed, the values in Table 1 agree with this added thermal resistance model.

4.5 Critical heat flux

CHF could not be measured for water due to the limitation of the power supply used, but it is calculated according to the equation of Lienhard and Dhir [38] to be about 200 W/cm^2 for a plain flat surface. CHF could also not be measured for the sintered+CNT surface with HFE-7300 working fluid because of plugging of the twin Graham-type condensers, which caused the pool pressure to begin to increase. Therefore heat flux beyond 26.4 W/cm^2 could not be imposed.

Values of critical heat flux for HFE-7300 are given in Table 1. In the fourth and fifth columns of the table, values of critical heat flux and wall superheat are compared to the CHF data point for the baseline bare copper surface. It is seen that CNTs alone do not significantly increase the maximum value of heat flux but do reduce the wall superheat at CHF by several degrees. CNTs added to the sintered copper matrix, however, result in a critical heat flux that is enhanced beyond the additive contribution of either structure by itself. Below, several quantitative models are investigated to help explain the CHF increases for HFE-7300.

The Lienhard and Dhir [38] modification of the Kutateladze-Zuber [39,40] critical heat flux,

$$q''_{CHF} = 0.149\rho_v^{1/2} h_{lv} \left[\sigma g(\rho_l - \rho_v)\right]^{1/4} \tag{3}$$

predicts a value of 17.8 W/cm^2 for HFE on the plain flat copper. This value agrees extremely well with the experimentally determined CHF. For the other surfaces, the following mechanisms are proposed for CHF enhancement in the boiling of HFE-7300, according to prevailing theories of departure from nucleate boiling (DNB):

1. Gross area enhancement
2. Forced modulation of the liquid-vapor instability at the dryout interface
3. Wettability increase
4. Capillarity increase

The area enhancement provided by the traditional sintered surface is difficult to determine for the nucleate boiling portion of the curve; for CHF, however, the enhanced area is that of the dryout interface. A geometric model of the dryout interface was developed considering both the exposed vertical sides of the porous coating and the horizontal area above it. A wavy interface is proposed due to the requirement that the effective dryout surface conform around the spherical copper particles at the top of the porous layer. The predicted critical heat flux is then:

$$q''_{w,CHF} = q''_{plain,CHF} \times \frac{A_{intf}}{A_{base}} \tag{4}$$

The wavy horizontal interfacial surface was approximated as:

$$z = \left(\frac{R_p}{0.2625\pi^2} \right) \cos\left(\frac{\sqrt{0.2625}\pi x}{R_p} \right) \cos\left(\frac{\sqrt{0.2625}\pi y}{R_p} \right) \tag{5}$$

Eq. (5) represents a surface having sinusoidal waves with equal periods in two dimensions. The wavelength $2R_p/\sqrt{0.2625}$ results from the calculated porous cell size. To arrive at this value, it was assumed that the porosity $\varepsilon = 0.65$ is produced by a unit prismatic cell with height d_p. The maximum possible wave amplitude $R_p/0.2625\pi^2$ results from the requirement that the maximum curvature must be no greater than the curvature of the particles; *i.e.*, the liquid-vapor interface nowhere touches the spherical particles. The maximum area increase due to the wrapping of the interface around the particles, calculated by numerical integration of Eq. (5), is 32.3%. The area increase due to the exposed vertical sides is 15.7%. Therefore the total

interfacial area increase lies somewhere between 15.7% and 48.0%. This range compares favorably with the experimental CHF enhancement of the porous surface, which is 33.7%.

Under this mechanism, the CNT-enhanced sintered surface would be expected to have a slightly larger increase in CHF than the plain sintered surface. Because of the improved wicking capability of the CNT array, the wavy interface might sustain a larger amplitude, and the CHF enhancement should lie at the high end of the range specified above.

Forced modulation of the interface instability as a mechanism for CHF increase was investigated by Liter and Kaviany [8] for novel structured surfaces, and numerically and experimentally for conventional sintered surfaces by Polezhaev and Kovalev [41]. Their predicted values for CHF were at least three times as high as in the present experiment.

Capillarity increase of structured surfaces may delay the departure from nucleate boiling because of the persistent intrusion of liquid into the boiling surface by capillary pressure forces. The capillary pressure increase of the fluid in a porous structure may be simply expressed as:

$$p_c = \frac{2\sigma \cos\theta}{R_h}, \tag{6}$$

where θ is the average contact angle and R_h is the average hydrodynamic radius. Equation (6) is most applicable to a capillary tube, where θ and R_h are easily defined. To first order, however, Equation (6) should give a sense for the amount of excess pressure in the liquid for the different surface structures in this work. The excess pressure results in the tendency of liquid to either penetrate into the porous matrix or remain separate from it.

The carbon nanotube structure features pore radii on the order of 30 nm to 1 μm, based on analysis of SEMs of as-grown and matted CNT arrays, respectively. The appropriate contact angles are considered to be those of HFE-7300 and deionized water on graphene. Values of θ must be assumed, since no information is available in the literature for contact angles on CNT

walls at elevated temperature. Based upon the work of Wang *et al.* [42] and Sullivan [43], we estimate the contact angles to be, to first order, 20° and 120° for HFE-7300 and DI water, respectively, at the saturation temperature.

The magnitude of the capillary pressure, according to Equation (6), will therefore be between about 20 and 600 kPa for HFE-7300. Capillary pressures in this range are quite high and could be responsible for significantly enhanced ability of the liquid to maintain contact with the boiling surface. For DI water, the negative value of cos(120°) means that water will not wick into the CNT array beyond the metallized tip under any circumstance.

The HFE-7300 boiling curves of Figure 3 are consistent with the capillarity predictions. Above a relatively low heat flux of 7 W/cm^2, the boiling curves for the CNT-enhanced sintered surface depart from those corresponding to the unmodified sintered surface. It is at this point (possibly the depth to which the CNT coating penetrates) that the plain sintered surface is believed to begin experiencing a significantly greater amount of dryout within the sintered layer than the hybrid surface. For the flat surfaces, the increased slope of the boiling curve for the CNT-enhanced surface suggests a higher boundary layer thermal conductivity, which may be explained by increased liquid contact with the surface. CHF is not greatly increased for the CNT-enhanced flat surface, however, implying that the hydrodynamic limitation still prevails.

The water boiling curves of Figure 4 also support the capillarity increase mechanism. The sintered surface curves with and without CNTs are virtually indistinguishable, which would be expected if water did not intrude into the CNT arrays. The flat surface heat transfer enhancement by CNTs can be attributed to the addition of a large number of nucleation sites provided by the spaces between nanotubes.

The enhanced wicking ability of the CNT-modified structures can be seen in the SEM photo in Figure 5. On the left-hand side of the image, a wetting liquid (rosin) has been drawn by the CNT mesh around the particles. The liquid interface depicted is similar to what might be expected from a highly wetting fluid such as HFE-7300.

4.6 Surface morphology change

One issue of concern with CNT-based nanostructures is their robustness with use. The CNT-enhanced boiling surfaces were inspected by SEM prior to soldering to the copper heater block, and again after desoldering from the heater blocks following testing. Before soldering and testing were performed, as shown in Figure 1(a), the CNTs appeared as individual tubes, partially aligned and also somewhat randomly intertwined. CNTs grown on the sintered particles were less aligned, but still individually distinguishable.

Following testing, the tubes appeared to have bundled into open-cell porous mats, as shown in Figure 6. The soldering/desoldering processes and pool boiling test all occurred at temperatures less than 200 °C. It is therefore unlikely that factors such as chemical changes are occurring, and instead, it is only the wetting associated with pool boiling that is responsible for the observed change in surface structure. Because SEMs were obtained only before and after all tests were conducted, it is unknown whether water, HFE-7300, or both were responsible for CNT matting. Other SEM images revealed degradation of the metallized coating for both the CNT and hybrid samples, resulting in collection of Cu nanoparticles in clumps at the tips of the CNT arrays.

Powell [22] studied many samples of the type used in these experiments and found that boiling and evaporation tests with water caused some surface morphology change, but did not find matting as drastic as observed here. It is therefore likely that the HFE-7300 working fluid

was mostly responsible for the observed deformation of the CNT array. Extreme bundling of MWCNTs has been previously observed after wetting by the highly wetting fluid isopropyl alcohol [44].

5 CONCLUSIONS

Pool boiling heat transfer enhancement by novel and more traditional porous surfaces was investigated for a highly wetting fluid, HFE-7300, and a less wetting fluid, deionized (DI) water. The surfaces consisted of a plain, flat copper surface, a sintered copper surface, a flat copper surface covered with an array of copper-metallized MWCNTs, and a sintered copper surface covered with an array of copper-metallized MWCNTs. Overall, the hybrid sintered/CNT surface exhibited the best boiling performance for both fluids, although the traditional sintered surface performed just as well for water. For HFE-7300, the hybrid surface achieved more than a 46% increase in CHF, while decreasing the wall superheat at CHF by 22.6% and the incipience temperature by 96% as compared to a plain flat surface. For water, CHF was not measured, but the incipience temperature was reduced by 95%.

The copper metallization layer, of 20 nm thickness, is believed to have partially separated from the CNTs during thermal testing, migrating in the form of nanoparticles at the array tips.

Pool boiling performance was most enhanced for the highly wetting fluid in conjunction with the sintered/CNT surface. Although the CNT array suffered deformation during testing, the CHF and h enhancements were nevertheless greater than the sum of the individual enhancements due to either a sintered layer or a CNT array. The increased performance was explained by both gross area enhancement and increased capillarity effects.

ACKNOWLEDGMENTS

Financial support for this work was provided by the Indiana 21st Century Research and Technology Fund and the Cooling Technologies Research Center at Purdue University. Justin Weibel assisted in fabrication of the boiling surfaces, and Anuradha Bulusu provided several SEM images. The authors also thank 3M Corporation and Delphi Electronics and Safety for providing fluid samples and related information.

REFERENCES

1. Y.Y. Hsu, On the Size Range of Active Nucleation Cavities in a Heating Surface, *Journal of Heat Transfer*, vol. 84, no. 3, pp. 207-216, 1962.
2. R.L. Webb, Nucleate Boiling on Porous Coated Surfaces, *Heat Transfer Engineering*, vol. 4, no. 3-4, pp. 71 - 82, 1983.
3. A. Czikk and P. O'Neill, 1979, Correlation of Nucleate Boiling from Porous Metal Films, in J.M. Chenoweth, J. Kaellis, J.W. Michel, and S. Shenkman (Eds.), *Advances in Enhanced Heat Transfer*, ASME, New York, pp. 103-113, 1979.
4. K. Nishikawa, T. Ito, and K. Tanaka, Enhanced Heat Transfer by Nucleate Boiling on a Sintered Metal Layer, *Heat Transfer-Japanese Research*, vol. 8, no. 2, pp. 65-81, 1979.
5. N.H. Afgan, L.A. Jovic, S.A. Kovalev, and V.A. Lenykov, Boiling Heat Transfer from Surfaces with Porous Layers, *International Journal of Heat and Mass Transfer*, vol. 28, no. 2, pp. 415-422, 1985.
6. C. Ramaswamy, Y. Joshi, W. Nakayama, and W.B. Johnson, Compact Thermosyphons Employing Microfabricated Components, *Microscale Thermophysical Engineering*, vol. 3, no. 4, pp. 273 - 282, 1999.
7. C. Ramaswamy, Y. Joshi, W. Nakayama, and W.B. Johnson, Effects of Varying Geometrical Parameters on Boiling from Microfabricated Enhanced Structures, *Journal of Heat Transfer*, vol. 125, no. 1, pp. 103-109, 2003.
8. S.G. Liter and M. Kaviany, Pool-Boiling CHF Enhancement by Modulated Porous-Layer Coating: Theory and Experiment, *International Journal of Heat and Mass Transfer*, vol. 44, no. 22, pp. 4287-4311, 2001.

9. M. Arik and A. Bar-Cohen, Effusivity-Based Correlation of Surface Property Effects in Pool Boiling CHF of Dielectric Liquids, *International Journal of Heat and Mass Transfer*, vol. 46, no. 20, pp. 3755-3764, 2003.
10. J.R. Saylor, An Experimental Study of the Size Effect in Pool Boiling CHF on Square Surfaces, Master's Thesis, University of Minnesota, Minneapolis, 1989.
11. W. Wu, J.-H. Du, and B.-X. Wang, Boiling Heat Transfer on Surfaces Coated by Porous Wick with Vapor Channels, *Microscale Thermophysical Engineering*, vol. 5, no. 4, pp. 277 - 284, 2001.
12. B.R. Alexander and E.N. Wang, Design of a Microbreather for Two-Phase Microchannel Heat Sinks, *Nanoscale and Microscale Thermophysical Engineering*, vol. 13, no. 3, pp. 151 - 164, 2009.
13. K.-J. Park and D. Jung, Boiling Heat Transfer Enhancement with Carbon Nanotubes for Refrigerants Used in Building Air-Conditioning, *Energy and Buildings*, vol. 39, no. 9, pp. 1061-1064, 2007.
14. K.-J. Park and D. Jung, Enhancement of Nucleate Boiling Heat Transfer Using Carbon Nanotubes, *International Journal of Heat and Mass Transfer*, vol. 50, no. 21-22, pp. 4499-4502, 2007.
15. K.-J. Park, D. Jung, and S.E. Shim, Nucleate Boiling Heat Transfer in Aqueous Solutions with Carbon Nanotubes up to Critical Heat Fluxes, *International Journal of Multiphase Flow*, vol. 35, no. 6, pp. 525-532, 2009.
16. V. Khanikar, I. Mudawar, and T. Fisher, Effects of Carbon Nanotube Coating on Flow Boiling in a Micro-Channel, *International Journal of Heat and Mass Transfer*, vol. 52, no. 15-16, pp. 3805-3817, 2009.

17. S. Launay, A.G. Fedorov, Y. Joshi, A. Cao, and P.M. Ajayan, Hybrid Micro-Nano Structured Thermal Interfaces for Pool Boiling Heat Transfer Enhancement, *Microelectronics Journal*, vol. 37, no. 11, pp. 1158-1164, 2006.
18. S. Ujereh, T. Fisher, and I. Mudawar, Effects of Carbon Nanotube Arrays on Nucleate Pool Boiling, *International Journal of Heat and Mass Transfer*, vol. 50, no. 19-20, pp. 4023-4038, 2007.
19. H.S. Ahn, N. Sinha, M. Zhang, D. Banerjee, S. Fang, and R.H. Baughman, Pool Boiling Experiments on Multiwalled Carbon Nanotube (MWCNT) Forests, *Journal of Heat Transfer*, vol. 128, no. 12, pp. 1335-1342, 2006.
20. S.S. Kim, J.A. Weibel, S.V. Garimella, and T.S. Fisher, Thermal Performance of Carbon Nanotube Enhanced Vapor Chamber Wicks, *14th International Heat Transfer Conference*, Paper No. IHTC14-22929, 2010.
21. M. Hashimoto, H. Kasai, H. Ryoson, K. Yazawa, J.A. Weibel, and S.V. Garimella, Nano-Structured Two-Phase Heat Spreader for Cooling Ultra-High Heat Flux Sources, *14th International Heat Transfer Conference*, Paper No. IHTC14-22765, 2010.
22. G.A. Powell, Controlled Synthesis of CNT-Based Nanostructures for Enhanced Boiling and Wicking, Master's Thesis, Purdue University, West Lafayette, Indiana, 2009.
23. J. Xu and T.S. Fisher, Enhancement of Thermal Interface Materials with Carbon Nanotube Arrays, *International Journal of Heat and Mass Transfer*, vol. 49, no. 9-10, pp. 1658-1666, 2006.
24. M. Meyyappan, L. Delzeit, A. Cassell, and D. Hash, Carbon Nanotube Growth by PECVD: A Review, *Plasma Sources Science and Technology*, vol. 12, no. 2, pp. 205-216, 2003.

25. P. Amama, B. Cola, T. Sands, X. Xu, and T. Fisher, Dendrimer-Assisted Controlled Growth of Carbon Nanotubes for Enhanced Thermal Interface Conductance, *Nanotechnology*, vol. 18, no. 38, p. 385303, 2007.
26. J.P. McHale and S.V. Garimella, Bubble Nucleation Characteristics in Pool Boiling of a Wetting Liquid on Smooth and Rough Surfaces, *International Journal of Multiphase Flow*, vol. 36, no. 4, pp. 249-260, 2010.
27. Fluent, Inc., Fluent 6.2 User's Guide, Fluent, Inc., Lebanon, NH, 2005, 2005.
28. S. Klein and F. Alvarado, Ees: Engineering Equation Solver for the Microsoft Windows Operating System, F-Chart software, Madison, Wisconsin, 1992-2010.
29. B.J. Jones and S.V. Garimella, Effects of Surface Roughness on the Pool Boiling of Water, *2007 Proceedings of the 5th Joint ASME/JSME Fluids Engineering Conference*, paper no. HT2007-32230, 2007.
30. V.P. Carey, *Liquid-Vapor Phase-Change Phenomena: An Introduction to the Thermophysics of Vaporization and Condensation*, Hemisphere Publishing Corp., Washington, D.C., 1992.
31. S.G. Bankoff, Entrapment of Gas in the Spreading of a Liquid over a Rough Surface, *American Institute of Chemical Engineers Journal*, vol. 4, no. 1, pp. 24-26, 1958.
32. S.G. Bankoff, A.J. Hajjar, and J.B.B. McGlothin, On Nature and Location of Bubble Nuclei in Boiling from Surfaces, *Journal of Applied Physics*, vol. 29, no. 12, pp. 1739-1741, 1958.
33. J.J. Lorenz, B.B. Mikic, and W.M. Robsenow, Effect of Surface Conditions on Boiling Characteristics, *Proc. 5th International Heat Transfer Conference*, vol. 4, Hemisphere, New York, pp. 35-39, 1974.
34. K. Cornwell, On Boiling Incipience Due to Contact-Angle Hysteresis, *International Journal of Heat and Mass Transfer*, vol. 25, no. 2, pp. 205-211, 1982.

35. Y. Qi and J.F. Klausner, Heterogeneous Nucleation with Artificial Cavities, *Journal of Heat Transfer*, vol. 127, no. 11, pp. 1189-1196, 2005.
36. S.J. Reed and I. Mudawar, Elimination of Boiling Incipience Temperature Drop in Highly Wetting Fluids Using Spherical Contact with a Flat Surface, *International Journal of Heat and Mass Transfer*, vol. 42, no. 13, pp. 2439-2454, 1999.
37. B.J. Jones, J.P. McHale, and S.V. Garimella, The Influence of Surface Roughness on Nucleate Pool Boiling Heat Transfer, *Journal of Heat Transfer*, vol. 131, no. 12, p. 121009, 2009.
38. J.H. Lienhard and V.K. Dhir, Hydrodynamic Prediction of Peak Pool Boiling Heat Fluxes from Finite Bodies, *Journal of Heat Transfer*, vol. 95, no. 2, pp. 152-158, 1973.
39. S.S. Kutateladze, On the Transition to Film Boiling under Natural Convection, *Kotloturbostroenie*, vol. 3, p. 10, 1948.
40. AECU-4439, California. Univ., Los Angeles; and Ramo-Wooldridge Corp., Los Angeles, Hydrodynamic Aspects of Boiling Heat Transfer, AECU-4439, California. Univ., Los Angeles; and Ramo-Wooldridge Corp., Los Angeles, 1959, 1959.
41. Y.V. Polezhaev and S.A. Kovalev, Modeling Heat-Transfer with Boiling on Porous Structures, *Therm. Eng.*, vol. 37, no. 12, pp. 617-620, 1990.
42. S. Wang, Y. Zhang, N. Abidi, and L. Cabrales, Wettability and Surface Free Energy of Graphene Films, *Langmuir*, vol. 25, no. 18, pp. 11078-11081, 2009.
43. D.E. Sullivan, Surface Tension and Contact Angle of a Liquid--Solid Interface, *Journal of Chemical Physics*, vol. 74, no. 4, pp. 2604-2615, 1981.

44. Z. Liu, N. Bajwa, L. Ci, S.H. Lee, S. Kar, P.M. Ajayan, and J.Q. Lu, Densification of Carbon Nanotube Bundles for Interconnect Application, *International Interconnect Technology Conference, IEEE 2007*, pp. 201-203, 2007.
45. 3M Corporation, 3M Thermal Management Fluids, 3M Corporation, St. Paul, MN, 2009, Document 98-0212-2649-7, 2009.
46. E. Lemmon, M. McLinden, and D. Friend, 2010, Thermophysical Properties of Fluid Systems, in P. Linstrom and W. Mallard (Eds.), *NIST Chemistry Webbook, NIST Standard Reference Database Number 69*, vol. 20899, National Institute of Standards and Technology, Gaithersburg MD, 2010.

NOMENCLATURE

A	area, m^2
d_p	particle diameter, m
g	acceleration due to gravity, m/s^2
h	heat transfer coefficient, $W/m^2 \cdot K$
h_{lv}	enthalpy of vaporization, J/kg
k	thermal conductivity, $W/m \cdot K$
n	boiling curve exponent
p	absolute pressure, Pa
r_c	cavity radius, m
R_h	hydrodynamic radius, m
R_p	particle radius, m
q''	heat flux, W/cm^2
T	temperature, K (unless °C is specified)
ΔT	temperature difference with respect to saturation, K or °C

Greek

δ	coating thickness, m
ε	porosity (fraction void), unitless
λ	wavelength, m
ρ_v	mass density of vapor, kg/m^3
ρ_l	mass density of liquid, kg/m^3
θ	liquid side contact angle, rad or °
σ	surface tension, N/m

Subscripts

b	bubble
base	base (area of heater block cross section)
c	capillary
CHF	at critical heat flux
crit	critical (or at critical point)
i	at incipience
in	input
intf	of the liquid-vapor interface
l	of liquid
loss	loss
min	minimum achieved
plain	of the plain flat surface
s	of solid
sat	at saturation
v	of vapor
w	of the heated wall
x	horizontal plane coordinate
y	horizontal plane coordinate
z	normal to surface coordinate
∞	of ambient

Table 1. Measured values of critical heat flux (CHF) for HFE-7300 in boiling tests.

Surface	$q''_{w,CHF}$ [W/cm^2]	$\Delta T_{w,CHF}$ [K]	CHF enhancement [%]	Wall superheat reduction at CHF [%]
Bare copper	18.1	23.4	–	–
CNT-enhanced	18.9	16.4	4.4	29.9
Sintered copper	24.2	38.6	33.7	- 65.0
Sintered copper + CNTs*	26.4	18.1	> 45.9	22.6

* Point of maximum measured heat flux (not CHF)

Table 2. Measured boiling incipience superheats for all surfaces and fluids tested, along with calculated incipient bubble radii. Values in table are the maximum single-phase wall superheats measured and accuracy is based upon the magnitude of the input power increment.

Surface	HFE-7300*		DI water†	
	$\Delta T_{w,i}$ [K]	$r_{b,i}$ [μm]	$\Delta T_{w,i}$ [K]	$r_{b,i}$ [μm]
Bare copper	22.5 ± 2.0	0.279 ± 0.026	9.7 ± 0.6	3.51 ± 0.22
Metallized CNT	12.6 ± 1.2	0.498 ± 0.049	4.8 ± 1.2	7.46 ± 1.89
Sintered copper	6.6 ± 2.3	1.07 ± 0.38	0.4 ± 0.1	88.6 ± 22.2
Sintered copper + metallized CNT	0.8 ± 0.2	8.27 ± 2.07	0.5 ± 0.2	79.2 ± 31.7

* Thermophysical property values estimated from [45]

† Thermophysical property values obtained from [46]

List of Figures

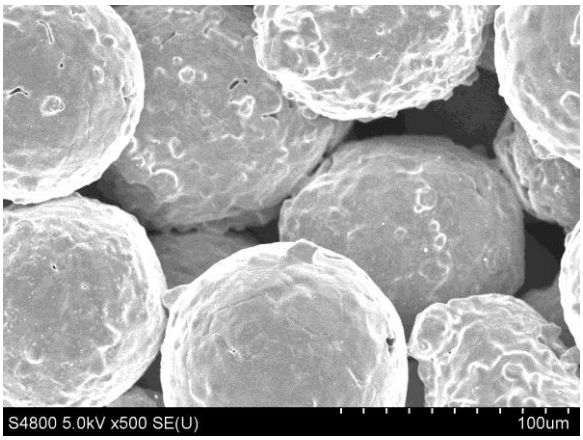

(a)

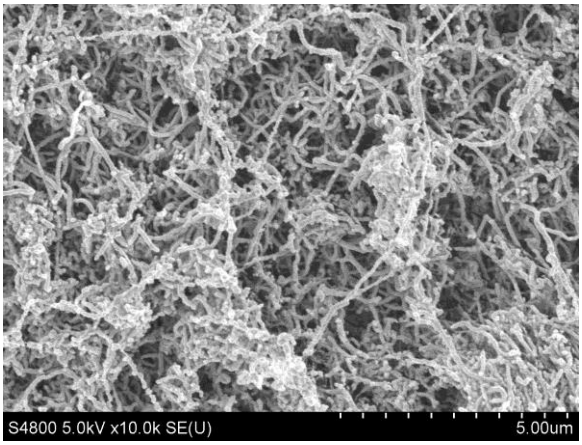

(b)

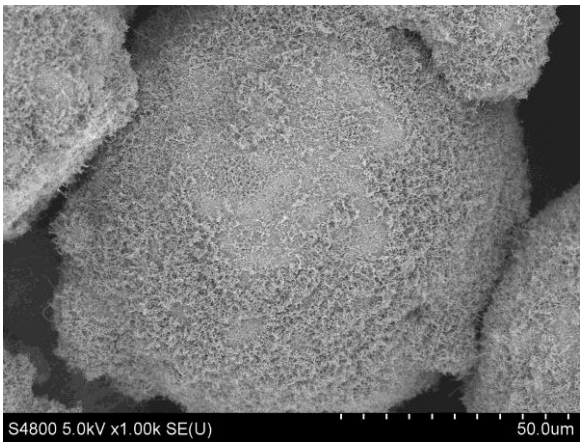

(c)

Figure 1. SEM images of boiling surfaces fabricated for this work: (a) porous layer formed of sintered copper spheres, (b) Cu-metallized MWCNT array, and (c) sintered Cu spheres with metallized CNT array grown after sintering.

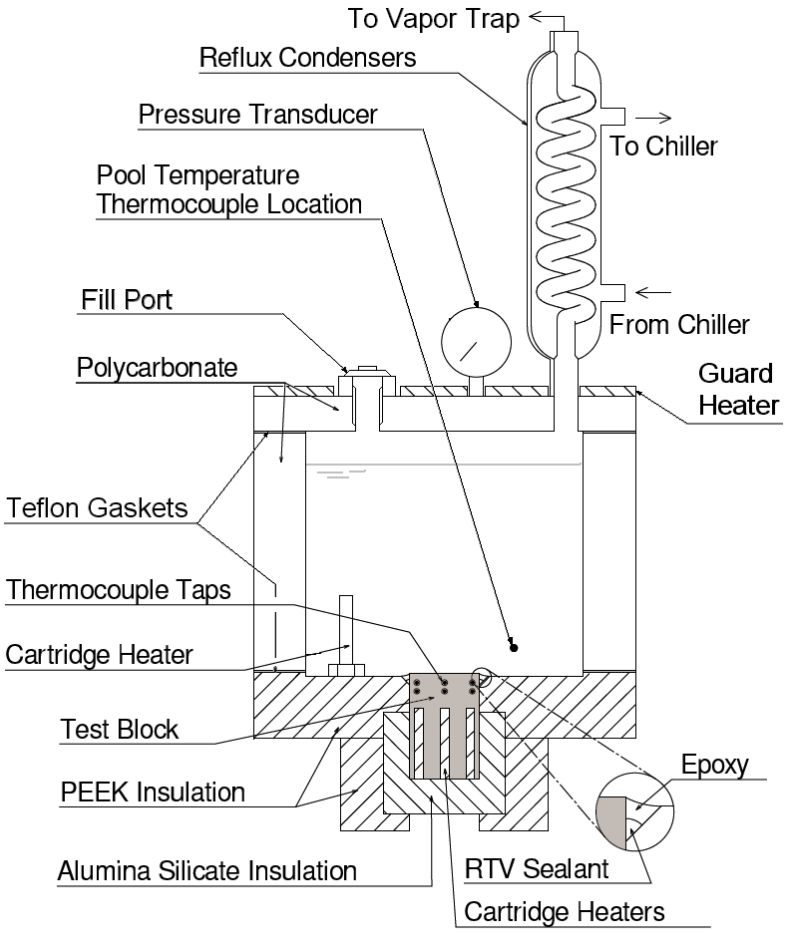

(a)

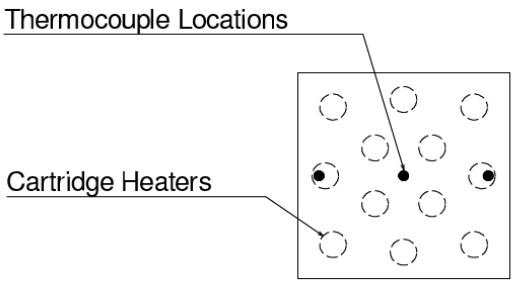

(b)

Figure 2. (a) Schematic diagram of the experimental facility with relevant components indicated, and (b) top view of the test block (adapted from [26]).

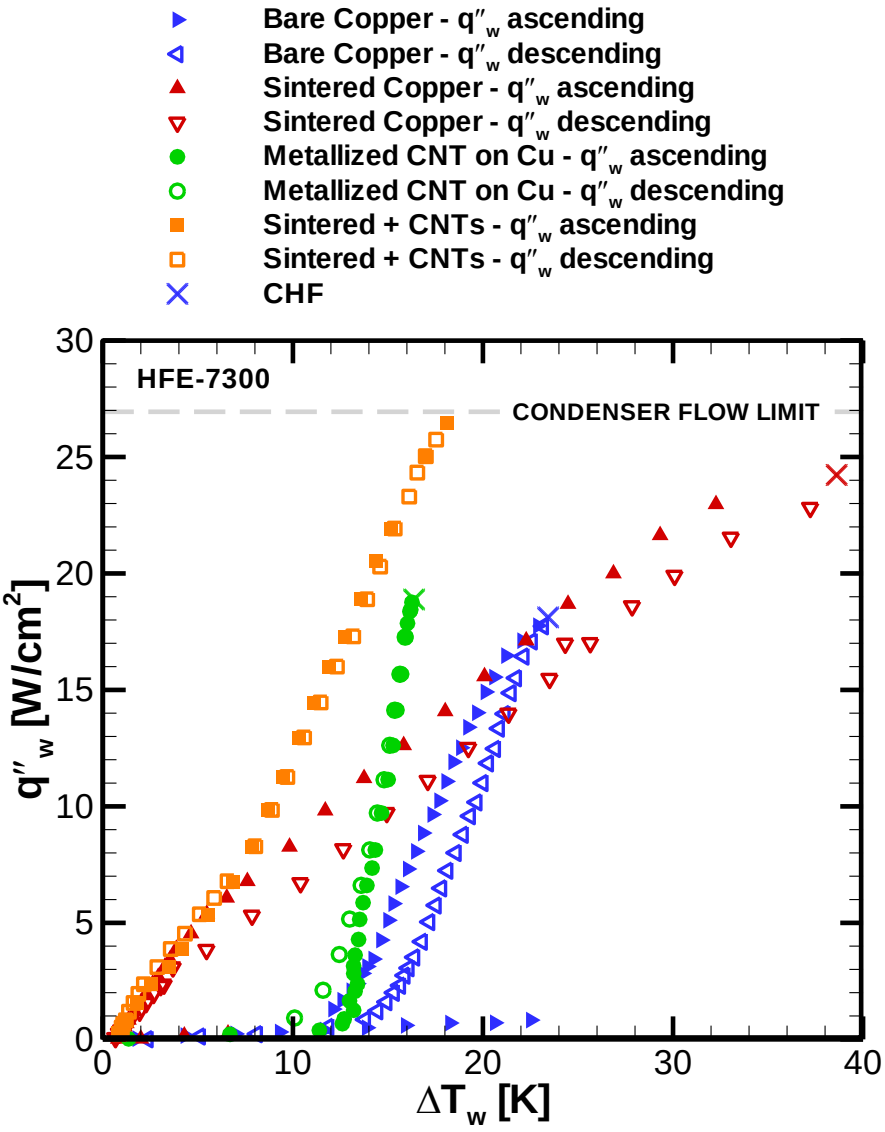

Figure 3. HFE-7300 pool boiling curves for the enhanced surfaces and the plain surface.

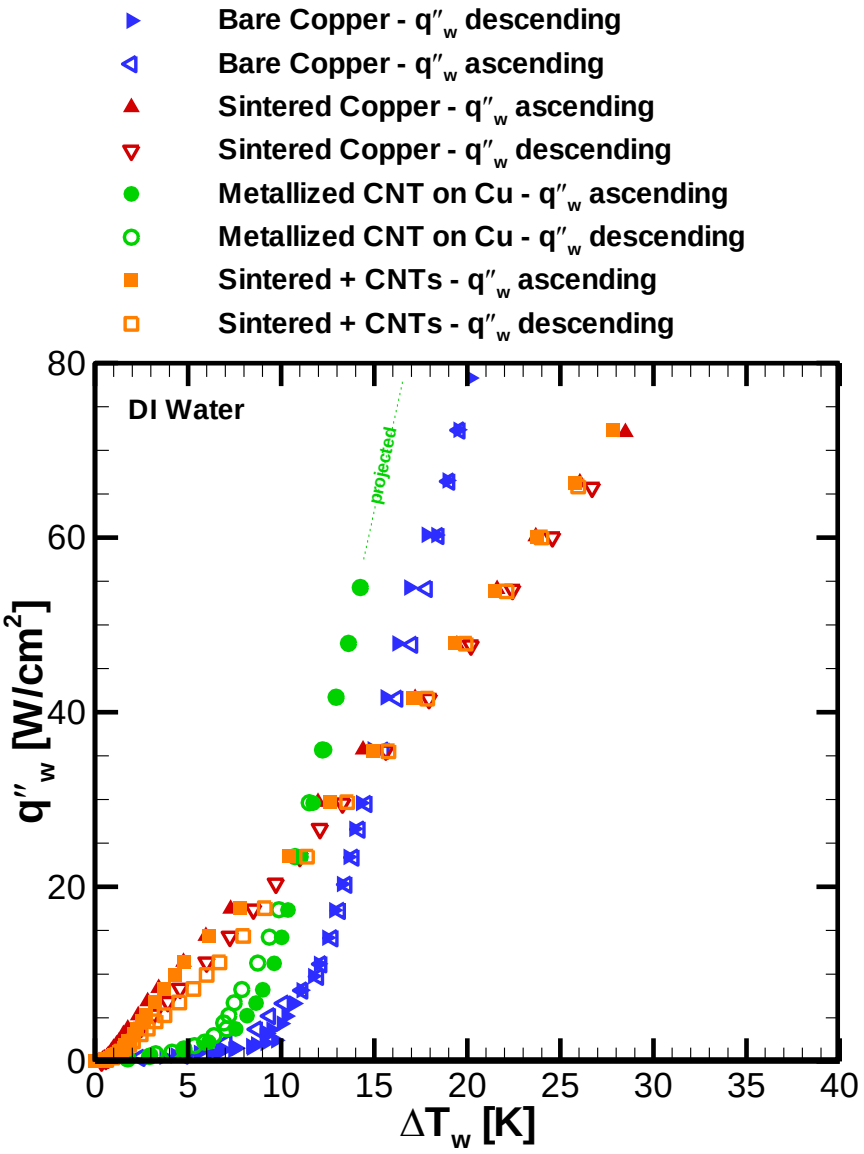

Figure 4. DI water pool boiling curves for the enhanced surfaces and the plain surface.

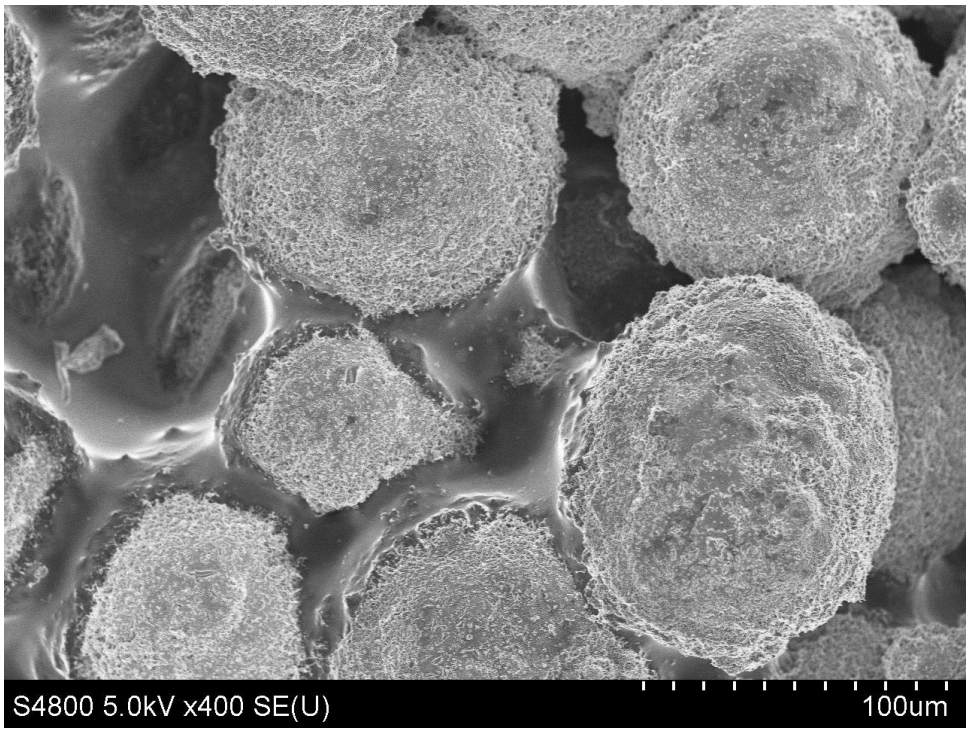

Figure 5. SEM image of a (resin) wetting front within the sintered copper-CNT porous matrix.

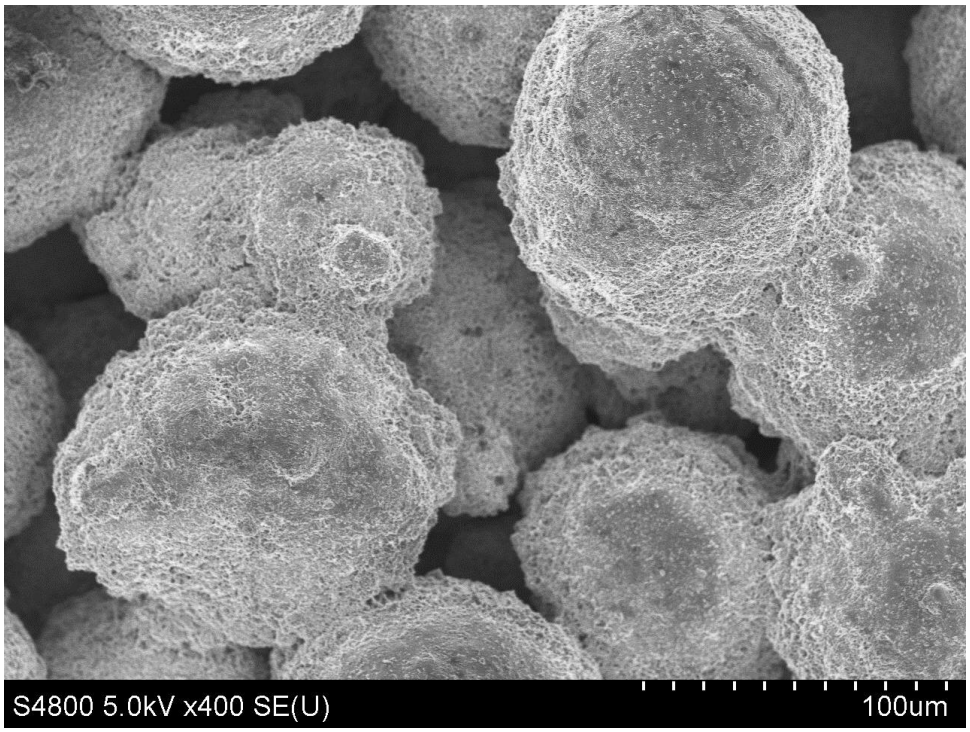

(a)

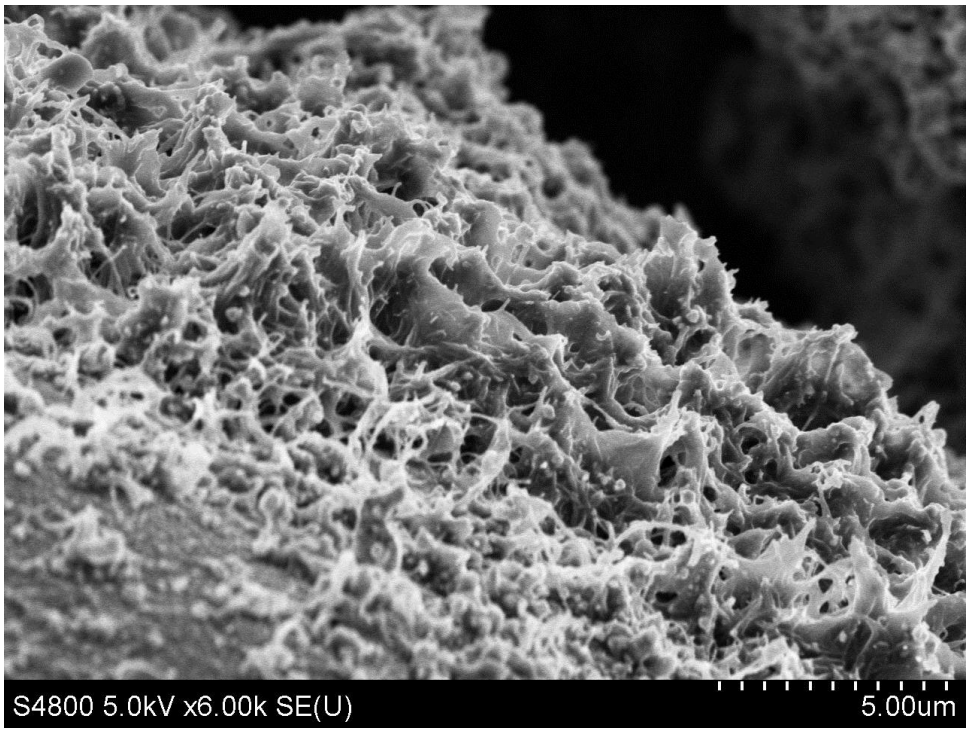

(b)

Figure 6. SEM images of the sintered boiling surface after pool boiling tests and desoldering.